

1 Pathways of the Agulhas waters poleward of 29°S

Jinbo Wang,¹, Matthew R. Mazloff,¹, Sarah T. Gille,¹

Manuscript has been accepted by JGR-oceans.
Low resolution figures are used in this document
to keep the PDF file small (<3M).
Jinbo Wang
June 12, 2014

Jinbo Wang, Scripps Institution of Oceanography, La Jolla, CA, 92122 (jinbow@alum.mit.edu)

¹Scripps Institution of Oceanography,
UCSD, La Jolla, California, USA.

2 **Abstract.** Passive tracers are advected in a Southern Ocean State Es-
3 timate (SOSE) to map the pathways of Agulhas waters, with a focus on de-
4 termining where the Agulhas waters intrude into the Antarctic Circumpo-
5 lar Current (ACC). Results show that Agulhas waters spread into all three
6 ocean basins within three years of release. After leaving the African conti-
7 nent the mean Agulhas water pathway tilts northwest toward the South At-
8 lantic and southeast toward the ACC. The majority (from 60% to 100% de-
9 pending on specific watermass) of the Agulhas waters stay in the South In-
10 dian Ocean north of the Subantarctic Front. From 10-28% enters the South
11 Atlantic Ocean through the boundary current along the southern tip of South
12 Africa and via Agulhas rings in the retroflexion region. Up to 12% of inter-
13 mediate depth Agulhas waters enters the ACC. Most of the tracer transport
14 into the ACC occurs just downstream of the Kerguelen Plateau, which clearly
15 demonstrates the importance of topography in elevating cross-frontal exchange.
16 Agulhas waters also contribute to Subantarctic Mode Water formation in the
17 Southeast Indian Ocean by lateral advection. The surface Agulhas waters
18 are pre-conditioned by strong surface buoyancy loss before turning into mode
19 water, while the intermediate Agulhas waters are advected to the mode wa-
20 ter formation region along isopycnals before being drawn into the mixed layer.

1. Introduction

21 The Agulhas Current, the swift boundary current along the southeast coast of the
22 African continent, is one of the major western boundary currents in the world oceans.
23 It carries warm and saline Indian, Arabian Sea, and Red Sea waters southward along
24 the southeast African coast [*Harris, 1972; Lutjeharms, 1976; Biastoch and Krauss, 1999;*
25 *Beal et al., 2006*]. It splits into two branches after passing the Agulhas bank. One
26 branch, the so-called Agulhas leakage, transports Indian Ocean waters into the south
27 Atlantic via energetic and intermittent Agulhas rings [*Richardson, 2007*]. This transport
28 of warm and saline Indian water by the Agulhas leakage is referred to as the “warm
29 water route” in the global conveyor belt schematic [*Gordon, 1986*]. It compensates the
30 southward export of the North Atlantic Deep Water (NADW) formed in the subarctic
31 North Atlantic and plays an important role in the global ocean circulation and climate
32 [*Beal et al., 2011; Caley et al., 2012*]. Recent studies have recognized that an increase
33 in Agulhas leakage could strengthen the Atlantic overturning circulation in response to
34 the poleward shift of the westerly jet in the Southern Hemisphere [*Biastoch et al., 2009a;*
35 *Beal et al., 2011; Biastoch and Böning, 2013*]. The majority of Agulhas waters do not
36 leak into the south Atlantic, but instead retroreflect back into the Indian Ocean to form the
37 Agulhas Return Current (ARC) [*Lutjeharms and Anson, 2001*], which flows eastward
38 along the subtropical convergence zone and interacts with the local atmosphere [*Large and*
39 *Yeager, 2009*]. The strong air-sea interaction is intimately linked to the Southern Annular
40 Mode (SAM) [*Sallée et al., 2010*] and to the formation of the Sub-Antarctic Mode Water
41 (SAMW) [*McCartney, 1982; Sallée et al., 2006*].

42 Because of the Agulhas waters' significant influence on the ocean circulation, mapping
43 its pathways is crucially important. The interactions between the ACC and the subtrop-
44 ical convergence are essential for the exchange of water masses between the subantarctic
45 and subtropical zones of the Southern Hemisphere, but the path of the ARC and its
46 interactions with the ACC are not well studied.

47 Here we use passive tracers integrated in a Southern Ocean State Estimate [SOSE,
48 *Mazloff et al.*, 2010] to map the pathways of Agulhas water originating at 29°S. The
49 results show that in addition to the Agulhas Leakage and the Agulhas Return Current,
50 the Agulhas waters flow southeastward and enter the ACC at several mixing hot-spots that
51 are instigated by topographic obstacles. The most notable intrusion into the ACC occurs
52 at the southwest Indian Ridge, the Crozet Plateau, and the Kerguelen Plateau (KP). The
53 Agulhas waters also seem to play an important role in the formation of SAMW.

2. Methodology

2.1. The SOSE

54 The high-resolution ($1/6^\circ$ by $1/6^\circ$) SOSE has been used extensively in studying the
55 Southern Ocean [*Mazloff et al.*, 2010]. SOSE is constrained to a large number of observa-
56 tions, including satellite altimetry and Argo profiling floats. The solution is optimized by
57 adjusting initial conditions, northern boundary conditions, and the atmospheric state. A
58 restoring open boundary layer is present between 24.7°S and 26.7°S, where the velocity,
59 temperature and salinity are nudged to prescribed values. It has little effect on the Agul-
60 has tracer transport as almost all the waters are transported southward at the beginning.
61 SOSE investigations have included evaluations of current structures [*Firing et al.*, 2011]
62 and watermass transformation [*Cerovečki et al.*, 2011, 2013], which are relevant to this

63 study. The assimilation analyzed here is carried out for three years from January 1, 2008
64 to December 31, 2010. It is denoted Iteration 60 and available at sose.ucsd.edu.

2.2. The Agulhas Current System in SOSE

2.2.1. Horizontal structure

66 The sea surface height (SSH) field in SOSE is comparable to that obtained from satellite
67 data. Figure 1 shows the time average and standard deviation of the SOSE SSH (right
68 panels) and satellite derived mean dynamic topography [*Paulis et al.*, 2012] (DOT08) and
69 standard deviation from AVISO (left panels) over the Agulhas current system regions for
70 the SOSE period (2008-2010). Similar to the conclusion in *Griesel et al.* [2012], the mean
71 dynamic topography in DOT08 is consistent with SOSE. The SSH is high in the South
72 Indian Ocean, and also in a narrow band in the Southeast Atlantic Ocean delineating
73 the mean pathway of the Agulhas leakage. Standing meanders are notable in the mean
74 dynamic topography, indicating the effect of topographic steering on the Agulhas Return
75 Current.

76 The standard deviation fields are similar in SOSE and AVISO. High SSH variability in
77 both products occurs over the Retroflexion region, the Agulhas Return Current, and the
78 Southwest Indian Ridge (30°E, 50°S), downstream of the KP, and along the northward
79 pathways that carries rings toward the Southeast Atlantic. The amplitude of the vari-
80 ability is slightly weaker in SOSE than in AVISO, but the structure is similar. Overall,
81 SOSE produces an SSH field similar to that observed by satellite.

2.2.2. Vertical structure

83 The Agulhas current in SOSE is similar in amplitude to previous studies and has a
84 reasonable structure. The cross section of the mean meridional velocity at 32°S (Figure

2 left) shows a V-shape as observed [Beal and Bryden, 1999]. The core of the southward
velocity exceeds 1 m s^{-1} centered about 60 km off the coast. The $1/6^\circ$ resolution in
SOSE marginally resolves the narrow boundary current but does not fully represent the
continental slope. As a result, the Agulhas undercurrent in SOSE is wider and less
constrained to the continental slope than observations indicate.

2.2.3. Volume transport

The transport of the Agulhas Current in SOSE, integrated along a zonal line at 32°S
extending 204km eastward from the coast, is consistent with observed values. The mean
southward volume transport is 65.9 Sv ($1\text{Sv}=10^6 \text{ m}^3 \text{ s}^{-1}$) with a standard deviation 14.6
Sv, and a 5-day-mean maximum and minimum 105.5 Sv and 34.7 Sv, respectively (Figure
3a). Bryden *et al.* [2005] estimated the 267-day averaged southward volume transport
across 32°S to be 69.7 ± 21.5 Sv. SOSE has a northward undercurrent transport of 2.5 ± 2.1
Sv (Figure 3b), similar to the 2.7 ± 2.6 Sv Agulhas undercurrent in a $1/10^\circ$ resolution
nested-domain simulation by Biastoch *et al.* [2009b]. These model undercurrent transports
are consistent but weaker than the 4.2 ± 2.9 Sv in Bryden *et al.* [2005] or the 4.2 ± 5.2 Sv
in Beal [2009]. The Agulhas undercurrent transport in SOSE becomes 5.0 ± 4.8 Sv if
integrated over 282 km from the coast. Both the northward and southward transports are
highly modulated by intermittent eddies, and show little seasonal variability.

2.3. Experiments with passive tracers

Since our assessment of the Agulhas Current System in SOSE shows it to be consistent
with observations, we carry out passive tracer experiments to map the pathways of the
Agulhas waters. Passive tracers are released on 01/01/2008 as a pulse along 29°S between
the South African continent and 42°E (yellow line in Figure 4). The section is chosen to be

107 11° wide in order to extend beyond the Agulhas Current and thus represents the greater
 108 Agulhas system. The sensitivity of our results to the tracer release initial condition is
 109 minimized both by releasing tracer at varying distances from the core of the Agulhas jet
 110 and by choosing initial conditions with a radius larger than the local eddy size or the
 111 width of the boundary current.

112 In total, sixteen tracers are used. Tracer #1 fills the entire section from surface to
 113 bottom (Figure 2 right panel). Another fifteen localized tracer patches are simultaneously
 114 released within the same section to assess individual pathways of the watermasses at
 115 different depths and offshore locations. Each of these fifteen tracers is initialized by

$$c(x_0, y_0, z_k) = \begin{cases} A \cos(\pi \frac{x-x_0}{dx} + 1) \cos(\pi \frac{y-y_0}{dy} + 1) f(z|z_k) & x_0 - dx < x < x_0 + dx; \\ & y_0 - dy < y < y_0 + dy \\ 0 & \text{elsewhere} \end{cases}$$

$$f(z|z_k) = \begin{cases} 1/[\Delta z_{k-1}, \Delta z_k, \Delta z_{k+1}] & z_{k-1} \leq z \leq z_{k+1} \\ 0 & \text{elsewhere,} \end{cases}$$

116 where in this case $dx = dy = 1^\circ$ is chosen, and $A = 1$ is chosen, though A can be an
 117 arbitrary value, and Δz_k represents the model layer thickness at the k_{th} vertical level.
 118 The tracers are advected online for three years from 2008 to 2010 as permitted by the
 119 SOSE duration. For this study, three years are sufficient, because after three years the
 120 Agulhas waters have been sufficiently modified such that they no longer retain their initial
 121 properties. The deep tracers are not transported southward within the three years studied,
 122 so are not discussed.

123 In order to quantify tracer transport, the SOSE domain is divided into 9 sectors sepa-
 124 rated by the gray lines in Figure 4, i.e., the south, north, and interior of the ACC in the
 125 Atlantic, Indian and Pacific Oceans. Here we choose the 20 Sv and 140 Sv time-mean

126 vertically integrated transport streamlines as proxies for the Polar Front (PF) and the
127 Sub-Antarctic Front (SAF), and to delineate the southern and northern ACC boundaries.
128 It may be optimal to define the fronts using instantaneous fields, but large uncertainties
129 exist due to energetic eddies. We analyze the tracer budget based on the last year time-
130 average which filters out the eddy fluctuations and expect the time-mean fronts to be more
131 appropriate than instantaneous fronts for this analysis. By defining the SAF as the ACC
132 boundary we only diagnose tracers that truly cross this front as being in the ACC, and
133 exclude tracers that reside on the northern flank of the front. The specific choice of the
134 ACC boundaries, however, does not affect the qualitative characteristics of the diagnosed
135 tracer pathways. Transport streamlines are calculated by vertically integrating and then
136 meridionally integrating the zonal velocity from south to north, with the zero streamline
137 defined to be the Antarctic coast. The South Atlantic and South Indian are separated by
138 the Good Hope line connecting the Cape of Good Hope and the 40°S parallel at 10°E.
139 This line is often used in the calculation of the Agulhas leakage [e.g., *Richardson*, 2007;
140 *Biastoch et al.*, 2009a; *van Sebille et al.*, 2010a]. The meridional line at 147°E connecting
141 the Antarctic continent to Tasmania and Australia separates the South Indian and South
142 Pacific oceans. By the end of the three-year simulation less than 2% of tracer #1 has been
143 lost through the northern boundary of the study domain in the Atlantic sector. Because
144 the lost tracer cannot reenter the SOSE domain, we renormalize the tracer concentration
145 at each time step in the analysis.

2.4. Watermasses

146 Sections 4 and 5 discuss tracer distribution in terms of watermasses including Sub-
147 Antarctic Mode Water (SAMW), Southeast Indian SAMW (SEISAMW), Antarctic In-

148 intermediate Water (AAIW), and Indian Ocean Sub-Tropical Mode Water (IOSTMW).
149 Here we follow the convention of *Talley et al.* [2011]. The associated temperature, salinity
150 and potential density for each watermass are listed in Table 1.

3. Horizontal tracer distribution

151 During the three-year integration the Agulhas waters are distributed broadly and reach
152 all three ocean basins. Figure 4 shows the 2010 time-averaged tracer #1 concentration,
153 integrated vertically, normalized by its maximum value and plotted on a logarithm scale.
154 The core tracer pathway stretches from the northwest to the southeast following the
155 Subtropical Front and the SAF through the Indian Ocean sector of the Southern Ocean.
156 Figure 4 shows that the ACC fronts and topography play multiple roles in shaping the
157 tracer pathways, acting as a barrier or as a mixer depending on the specific location. In
158 Sections 3.1 to 3.3, we describe the tracer distribution in the three ocean basins.

3.1. The South Atlantic Ocean

159 At the end of the three year integration, 9.9% of Tracer #1 has entered the South
160 Atlantic Ocean. This is not the conventional fraction of the Agulhas Leakage as Tracer #1
161 samples a large area beyond the Agulhas Current. After entering the South Atlantic from
162 the Agulhas Retroflection, the tracer is blocked from being advected further southwest
163 first by the SAF (indicated by a significant drop in tracer content) and second by the
164 Mid-Atlantic Ridge at 0°E. The tracer is largely confined to the north of 51°S at 0°E. To
165 the north of 40°S, however, steep topography, including the Walvis Ridge and the Mid-
166 Atlantic Ridge, play no detectable role in shaping the tracer pathways, as also noted in
167 previous studies [*Boebel et al.*, 2003; *Richardson*, 2007]. Some of the tracer reaches the east

168 coast of South America and is transported poleward by the Brazil Current, subsequently
169 crossing the SAF at the Brazil-Malvinas confluence.

3.2. The South Indian Ocean

170 At the end of 2010, 84.1% of tracer #1 remains in the south Indian Ocean north of
171 the SAF and 5% has entered the ACC. Tracer concentration is high in the Mozambique
172 Channel (around 40°E, 30°S), indicating the stagnant deep water in the channel. The
173 Crozet Basin between the Southwest Indian Ridge and the Southeast Indian Ridge traps
174 a large amount of tracer. The tracer is first mixed into the ACC around the Southwest
175 Indian Ridge and the Crozet Plateau at (40°E, 45°S). A small portion of the mixed tracer
176 passes the PF, enters the Enderby Basin and the Weddell Gyre around (40°E, 60°S), and
177 travels westward along the Antarctic coast. A more significant cross-ACC transport occurs
178 downstream of the KP at 70°E. The majority of this water is transported downstream
179 within the ACC. This striking cross-ACC transport is consistent with the finding of a
180 uniform potential vorticity pool downstream of the KP [*Thompson et al.*, 2010], caused
181 by enhanced eddy induced mixing. The tracer content decreases sharply to the south of
182 the PF.

3.3. The South Pacific Ocean

183 By the end of the three-year integration, 1% of Tracer #1 has entered the South Pacific.
184 The tracer is confined to the north of the PF. This is especially clear to the south of
185 Tasmania (near 150°E, 60°S), where both the PF and the tracer pathway are deflected
186 by the Southeast Indian Ridge. High tracer content straddles the SAF, which does not

187 appear to be a barrier to Agulhas waters because of the tracer mixing into the ACC
188 upstream of the KP.

3.4. The effect of Kerguelen Plateau

189 As a further demonstration of the significance of the topographic effect, we plot a
190 Hovmöller diagram of the vertical profile of the tracer concentration at five locations up
191 and downstream of the KP (Figure 5). Upstream of the KP (Figure 5a) tracer crosses
192 the ACC only 5 times during the three-year period with a very short duration in each
193 event. This means that, although infrequent, the tracer can be advected into this region
194 by sporadic eddies.

195 Immediately upstream of the KP (Figure 5b), one significant tracer intrusion event
196 occurs around month 24, i.e., two years after the tracer release. One notable feature is
197 the deep tracer near 1000 meters. This deep tracer is not a result of the local subduction
198 of the upper-level tracer, because tracer appears much earlier in the deeper layer (at
199 month 19) than in the upper layer (at month 23). The tracer concentration shows long
200 persistence with small temporal variability, indicating that the tracer is transported from
201 the north/northwest to this location by the mean boundary current along the western
202 boundary of the plateau. The tracer that appears around 1300 meters during the second
203 half of the third year may also have been advected from the north/northwest upstream.
204 Low concentration of tracer is found on the KP shelf due to the surface Ekman transport
205 being northward (Figure 5c).

206 In contrast to the region upstream of the KP (Figure 5a,b), tracer appears much more
207 frequently and with a much larger concentration downstream (Figure 5d,e). Tracer re-
208 leased near the surface requires 15 months to reach the region downstream of the KP,

209 while the transit time for tracer released deeper is longer. The tracer transport appears
210 to be more intermittent at site d than at site e, suggesting that the tracer at site d is
211 brought by eddies but that the tracer has been homogenized before reaching site e. Among
212 the five sample sites, the largest tracer concentration occurs at site e, downstream of the
213 KP.

4. Vertical tracer distribution

214 Pathways differ by density class and cannot be studied solely from a uniform surface-
215 to-bottom tracer release. Hence we also analyzed the 15 additional tracers that were
216 released in localized positions. Their depths and longitudes are indicated by the pie
217 charts in Figure 6. Over the three-year simulation more than 60% of the waters in the
218 Agulhas system remain in the South Indian Ocean north of the ACC (IN), and for deep
219 water originating in the Mozambique Channel almost 100% remains in IN (Figure 6, IN).
220 Intermediate waters originating between 400 and 1500 meters are more readily transported
221 out of the Indian Ocean than were the surface waters. This is especially true for water
222 originating close to the African continent. Up to 28% of intermediate water enters the
223 South Atlantic Ocean (AN), and about 12% ends in the Indian sector of the ACC (IA).
224 As surface water is advected faster than deep waters, most of the tracer that ends in the
225 Pacific was released in the upper ocean. The partition is relatively independent of the
226 offshore distance, which corroborates the results of *van Sebille et al.* [2010b].

227 Based on watermass properties and horizontal distributions, we split the tracers shown
228 in Figure 6 into three groups. The surface tracer refers to the ensemble of the upper six
229 tracers (0-400 m), the intermediate tracer refers to the middle six tracers (400-1500 m),

230 and the deep tracer refers to the deep three tracers. The deep tracers are not transported
 231 southward so are not discussed further.

232 The vertically integrated surface and intermediate tracer contents are shown in Figure
 233 7ab. The white lines are the mean tracer pathways defined as the tracer first moment in
 234 y ,

$$y_c = \frac{\int y \langle c \rangle^{z,t} dy}{\langle c \rangle^{y,z,t}}, \quad (1)$$

235 where we use the angle brackets to represent integration, i.e., $\langle c \rangle^{z,t} = \int \int c \, dz dt$. The sur-
 236 face and intermediate tracer distributions share a qualitatively similar large-scale feature
 237 with a northwest-southeast tilt. The main surface pathway is shifted northward relative
 238 to the main interior pathway due to surface northward Ekman flow (compare the relative
 239 shift of the two white lines to the location of the SAF in Figure 7ab).

240 The properties of the vertical tracer distribution are measured by the first moment, A_c ,
 241 and the second moment, σ_A , with respect to a chosen variable A ,

$$A_c(x, y, t) = \frac{\langle Ac \rangle^z}{\langle c \rangle^z} \quad (2)$$

and

$$\sigma_A^2(x, y, t) = \frac{\langle c(A - A_c)^2 \rangle^z}{\langle c \rangle^z}.$$

242 The first and second moments represent the local center and thickness of a specific
 243 tracer in A space. For example, if A represents the vertical coordinate z , the first moment
 244 represents the tracer mean depth and the second moment represents the the tracer spread
 245 in the vertical.

246 Figure 7 shows the first moment of the surface (c,e,g) and intermediate (d,f,h) tracer in
247 depth (c,d), neutral density (e,f) and salinity (g,h) space averaged over the last year. The
248 results are organized and presented for three different regions, i.e., the South Atlantic,
249 the South Indian Ocean to the north of the ACC (IN), and the Indian Ocean sector of
250 the ACC (IA).

4.1. The main pathway in the Indian Ocean

251 By the end of the the three-year model integration, the surface tracers have drifted
252 northward, carried by the surface Ekman flow. As a result, there is less surface tracer
253 than intermediate-level tracer within the Retroflexion region (Figure 7ab). The surface
254 tracer deepens to about 300 meters along the pathway in the Indian Ocean sector. The
255 deepening over the southeast Indian region coincides with the deep mixed-layer region,
256 suggesting that the tracer is mixed downward by the winter deep convection.

257 The main pathway going through the deep mixed-layer region indicates that waters are
258 modified, or pre-conditioned, by air-sea fluxes as they travel along the Agulhas Return
259 Current to the SAMW pool. The tracer gradually becomes denser (Figure 7e) and fresher
260 (Figure 7g) along this southeastward pathway, eventually contributing to the SAMW
261 formation via lateral advection. Upon reaching the location where the SEISAMW is
262 found vertical mixing spreads the tracer over a thicker depth range (Figure 8a), making
263 it more uniform in density (Figure 8c).

264 Tracers initiated in intermediate layers (Figure 7d) enter the Agulhas region at deeper
265 levels than the surface tracers (Figure 7e), but the intermediate-level tracers gradually
266 rise as they move toward the south Pacific. Intermediate tracers are advected mostly
267 along isopycnals indicated by the constant density along the main pathway (Figure 7f).

268 The main pathway of the intermediate tracers merges with the SAF to the east of 80°E ,
269 meaning that the SAF does not inhibit cross-frontal exchange. As a result of cross-frontal
270 exchange intermediate tracers become less saline as they move southeastward along the
271 main pathway (Figure 7f). By the time they reach the southeast Indian Ocean, surface
272 and intermediate tracers share the same depth and density ranges, suggesting that both
273 contribute to the SAMW formation.

274 The surface-originating tracers are found to the north of the SAF over the southeast
275 Indian Ocean (Figure 7c), while intermediate tracers straddle the SAF (Figure 7d). This
276 is because most of the surface tracers are constrained to the north of the SAF and become
277 well mixed in the pool of SAMW, while the core of the intermediate tracers coincides
278 with the SAF (Figure 9). As a result, the surface tracers occupy a thick depth range
279 along the main pathway, but they are compact in density space (Figure 8b, 9). For the
280 intermediate tracers, the lack of an obvious cross-SAF gradient downstream of the KP
281 suggests that SAF and the associated eddies act as a blender to stir intermediate waters
282 across the front (Figure 8b, 9). As shown in Figure 9, both the surface and intermediate
283 tracers contribute to the SAMW within the southeast Indian Ocean.

4.2. The South Atlantic Ocean

284 The tracers are advected into the South Atlantic and remain north of the SAF for both
285 the surface and intermediate levels (Figure 7ab). The main pathways defined by the first
286 moment in y extend northwestward suggesting the pathway of the Agulhas Leakage as
287 previously discussed [Richardson, 2007]. After entering the South Atlantic, both surface
288 and intermediate tracers shoal (Figure 7cd) due to the shallower isopycnals in the South
289 Atlantic Ocean. The tagged waters also become denser (Figure 7ef) due to the surface

290 cooling over the retroreflection region (Figure 10) and eddy induced mixing with ambient
291 Atlantic waters, and less saline (Figure 7gh). The large tracer spread in density space in
292 the South Atlantic Ocean (Figure 8cd) is a continuation of the large spread in the South
293 Indian recirculation region, indicating that the tracers have been extensively mixed before
294 entering the South Atlantic Ocean.

4.3. Cross frontal transport

295 Tracer intrusion into the ACC primarily occurs downstream of the KP. Some intrusions,
296 however, are also apparent at the Crozet Plateau region (Figure 7ab). Over this Crozet
297 Plateau region, the surface tracer content drops sharply to the south of the SAF, indicating
298 that local fronts block the southward advection of surface tracers. The streamfunction-
299 based SAF approximately matches the tracer contour, suggesting that the SAF acts as a
300 barrier over this region. Note, however, that the true barrier may be one of several strong
301 fronts that exist in the region, including the Crozet Front [*Pollard and Read, 2001*]. In
302 addition, the Polar Front can sometimes extend further north in this region [*Orsi et al.,*
303 *1995; Belkin and Gordon, 1996*].

304 Nevertheless some tracer does enter the ACC in this region, with intermediate depth
305 tracers being more readily mixed into the ACC than surface tracers (Figure 7b). This
306 tracer intrusion occurs at several hotspots, i.e., the southwest Indian ridge where inter-
307 basin exchange was observed previously [*Pollard and Read, 2001*] and the deep channel
308 between the Crozet Islands and the Kerguelen (Figure 8ab). Once these tracers enter the
309 ACC they mix, becoming denser and moving deeper in the water column (Figure 7cdef).
310 The stark meridional contrast in the tracer density and depth indicates that tracers have
311 entered the deeper layers of the ACC. Some of these tracers are then advected downstream

312 of the KP through, the Fawn Trough and they then flow along the southern ACC boundary
313 (Figure 7cdef and 8ab). The cross-KP flow through the Fawn Trough is a well observed
314 feature [Roquet *et al.*, 2009].

315 One caveat, however, is that the tracer content is low within this region resulting in
316 large uncertainties in the quantification of this pathway. Nevertheless, the results point out
317 an interesting cross-front exchange process and confirm the importance of the southwest
318 Indian Ridge in inter-basin exchanges.

319 Downstream of the KP the tracers are first transported into the ACC by a train of eddies
320 that emerge from the SAF to the north of the Plateau at 70°E (refer to the supplemental
321 movies). The majority of the tracers remain to the north of the PF. At the end of the
322 three-year run the surface-originating tracer that remains in the ACC is still shallower
323 than about 300 meters (Figure 7c). This tracer is now found largely in a pool of water
324 with neutral density around 27.0 ± 0.2 (Figure 7e) especially during austral winter time
325 which is marked by the red-black color in Figure (9ab), and it clearly shows an upper
326 layer salinity front (Figure 7g).

327 Tracers originating at intermediate depths are transported southeastward mainly by the
328 ACC primarily along the core of the SAF, as suggested by the coincidence of the tracer
329 concentration maximum and the SAF (Figure 9 blue contours). To the north of the SAF,
330 tracers are mixed into the mode water pool, indicated by the vertical homogenization of
331 tracers across density levels. To the south of the SAF, tracers are advected along isopyc-
332 nals indicated by the similar shape of tracer contours and isopycnals. The coincidence
333 of the local maximum in tracer concentration with warm-core eddies (the local deepening
334 in isopycnal contours) is a sign that eddies are involved in the southward and upward

335 transport of tracer, as discussed in the residual mean formulation [*Marshall and Speer,*
336 2012, and the references therein].

337 The phenomenon of tracer being advected to the south and mixed to the north of
338 the SAF is consistent with the regional potential vorticity (the lower panel of Figure 4).
339 Downstream of the KP, the main pathway of the intermediate tracers merges with the
340 SAF and bisects the low potential vorticity pool of the SEISAMW and the higher potential
341 vorticity ACC water. The tracers north of the main pathway are modified and blended
342 into the low potential vorticity pool. That they originated as high potential vorticity
343 waters means they counteract the mode water formation processes. Meanwhile, the lack
344 of mixing of tracers south of the SAF allows persistence of the high potential vorticity
345 signature. Furthermore, this pathway points to the importance of waters originating in
346 the Agulhas Current in explaining the relatively high potential vorticity signature found
347 over much of the ACC.

348 To summarize, the main pathways of the Agulhas waters are oriented along a northwest
349 to southeast axis. Surface initialized tracers are shifted northward relative to intermediate
350 depth initialized tracers because of surface Ekman transport. West of 80°E, the pathways
351 are centered north of the SAF. The SAF acts as a barrier upstream of the KP blocking
352 direct tracer mixing into the ACC from the subtropical region, with an exception of the
353 southwest Indian ridge and the deep channel between the Crozet Islands and the KP where
354 tracers leak into the ACC at depth. Downstream of the KP (east of 80°E), the SAF acts as
355 a blender, mixing tracers into the ACC. A significant amount of Agulhas waters reach the
356 SEISAMW formation region. Before reaching this area, surface waters experience strong
357 surface cooling within the Agulhas Retroflexion and the Agulhas Return Current regions

358 (Figure 10). In contrast intermediate waters remain approximately on the same isopycnal.
 359 Both processes strongly suggest the importance of lateral advection and pre-conditioning
 360 of the Agulhas waters to facilitate the SEISAMW formation.

5. Watermass modification

361 Agulhas waters are transformed as they spread, as is also observed in other modeling
 362 studies [e.g., *van Sebille et al.*, 2010a]. Here we use the tracers to mark the Agulhas waters
 363 and study their evolution. The first question is how quickly the Agulhas waters transform.
 364 Watermass transformation is reflected in the heat and salt content of the waters marked
 365 by the tracers. We use the tracer-weighted potential temperature, a proxy for tracer heat
 366 content, to investigate the time scale of watermass transformation,

$$\theta_c(t) = \frac{\langle \theta c \rangle^{x,y,z}}{\langle c \rangle^{x,y,z}},$$

where θ is potential temperature referenced to 0 pressure. The true heat content of a
 tracer is

$$H_c(t) = \rho c_p \langle c \rangle^{x,y,z} \theta_c(t),$$

367 where c is tracer concentration, ρ density, c_p the specific heat capacity for sea water,
 368 and H_c the tracer heat content. The tendency of the tracer temperature consists of two
 369 parts

$$\frac{\partial \theta_c}{\partial t} = \left\langle c \frac{\partial \theta}{\partial t} \right\rangle^{x,y,z} + \left\langle \theta \frac{\partial c}{\partial t} \right\rangle^{x,y,z}.$$

370 where c is normalized by $\langle c \rangle^{x,y,z}$. The first term on the right-hand side represents the
 371 influence of the temperature change of the water parcel marked by tracers. The second

372 term represents the change due to the tracer spreading into different temperature ranges.
373 For instance, if a tracer is stagnant, then $\partial c/\partial t = 0$, and the change of the tracer-weighted
374 temperature is solely due to the heat in and out of the tracer marked waters by surface
375 forcing or diffusion. Similarly, if a temperature field is stationary, the tracer temperature
376 change is solely because the tracer spreads into regions with different temperatures. In
377 our case both make measurable contributions.

378 We calculate the evolution of the tracer temperature based on Tracer #1 (Figure 11).
379 The total tracer volume is conserved within 98.8% (panel a). 1.2% is lost through the
380 northern boundary. The tracer weighted temperature continuously decreases (panel b),
381 due to the initial high potential temperature of the Agulhas waters. Most of the watermass
382 modification happens during the first 7 months, after which the tracers quasi-equilibrate
383 with the ambient atmosphere and ocean. Subsequent changes are due primarily to air-sea
384 flux as indicated by the clear seasonal cycle in $\partial\theta_c/\partial t$ (panel c).

385 We use the other 15 tracers to analyze the evolution of different watermasses in T-S
386 space (Figure 12). Near-surface Agulhas waters transform quickly as they flow southward.
387 The tropical surface waters originating at potential density level 23.5 kg m^{-3} (referenced
388 to the surface and following the standard procedure of subtracting 1000 kg m^{-3}) are
389 transformed to a density of 25.5 kg m^{-3} in less than 6 months (thick red in Figure 12a).
390 These waters continue to become denser, reaching a potential temperature of 14-15°C,
391 salinity of 35.3-35.4, and potential density of $26.2\text{-}26.3 \text{ kg m}^{-3}$ (red dots in Figure 12f).
392 At this density, the water is consistent with a mixture of IOSTMW and SAMW [*Beal*
393 *et al.*, 2006; *Cerovečki et al.*, 2013]. The quick initial transformation of the surface water
394 is primarily caused by surface heat loss as the temperature decreases sharply (Figure 12f)

395 red), but the salinity is relatively unchanged. Mixed-layer dynamics play a role in evolving
396 the waters in the upper 500 m, and the seasonal cycle is apparent in Figure 12a-c.

397 The tracer released at 438 meters has an initial potential density of 26.6 kg m^{-3} , po-
398 tential temperature 13.2°C , and salinity of 35.3. This water freshens and cools as it flows
399 adiabatically southeastward, indicating an interior along-isopycnal mixing with the ACC
400 waters.

401 Intermediate waters originating at 772 meters initially have a potential density of 27.3 kg
402 m^{-3} (Figure 12d, thick purple), but quickly mix with upper-layer waters becoming warmer
403 and saltier. They enter the ARC with a potential density of approximately 27.0 kg m^{-3}
404 and then flow adiabatically southeastward and experience little change in properties. They
405 do, however, become slightly colder and fresher indicating some along-isopycnal mixing
406 with ACC waters.

407 The intermediate Agulhas waters that reach the ACC (Figure 12e-f) experience large
408 mixing amplified by eddies generated from topographically induced instabilities. The
409 waters have density 26.5 kg m^{-3} upon entering the ACC, and eventually cool and freshen,
410 so that they can be characterized as AAIW. Meanwhile, deep waters initialized in the
411 Agulhas Current below 2000 meters are relatively stagnant (black dot in Figure 12f).

412 All waters that enter the South Atlantic experience dramatic transformations (thin lines
413 in Figure 12a-d and dots in Figure 12g). The Agulhas surface waters travel for about two
414 months before reaching the Agulhas Bank and entering the South Atlantic (Figure 12a-
415 b). These waters mix with subsurface waters and evolve for about a year until reaching a
416 point where they begin to oscillate around a density of approximately 26 kg m^{-3} (Figure
417 12a-b, g). The intermediate waters become warmer and saltier after entering the South

418 Atlantic Ocean (Figure 12c, g) due to strong turbulent mixing with upper waters at the
419 retroflection region and upwelling in the Benguela Current (figure not shown).

420 Based on a detailed sub-domain diagnoses of the tracer content in year-2010 and on
421 the evolution of tracer transport during the three-year simulation (detailed in Appendix)
422 we infer a schematic (Figure 13) showing the pathway of Agulhas waters over two main
423 levels, surface (0-400m, red) and intermediate (approximately 400-1500m, blue). The
424 main pathways of the Agulhas water at these two levels show a clear meridional offset,
425 with the surface waters shifted equatorward due to the northward Ekman transport. Hot
426 spots of cross-frontal transport of Agulhas waters, which exist in both levels but are more
427 prevalent in the intermediate level, occur at the retroflection region, the Southwest Indian
428 Ridge, and the Agulhas, Crozet and KPs. Most of the cross-ACC tracer mixing occurs
429 at these hot spots, with the location downstream of Kerguelen being the most significant.
430 A small amount of tracer crosses the Polar Front and is advected towards the Antarctic
431 Shelf.

6. Summary

432 The Agulhas Current system transports heat and salt from the Indian Ocean into the
433 South Atlantic and Southern Oceans. In this study, less attention has been paid to the
434 effect of the Agulhas leakage which is extensively discussed elsewhere [*Beal et al.*, 2011,
435 and the references therein]; instead, we focus on the southeast pathways of Agulhas waters
436 and find that the contributions of the Agulhas waters to the SEISAMW and the ACC
437 water are not negligible.

438 Using SOSE we carry out a series of passive tracer experiments initialized within an
439 11°-wide zonal section at 29°S to map the pathways of water originating in the Agulhas

440 current system. For the last year of the three-year run, we find that the majority (from
441 60% to 100% depending on specific watermass) of the Agulhas waters stay in the South
442 Indian Ocean north of the SAF, 10-28% enter the South Atlantic Ocean through the
443 boundary current along Africa and via Agulhas rings in the retroflexion region. Up to
444 12% of Agulhas Current intermediate water enters the ACC in the South Indian Ocean.

445 Significant amounts of Agulhas waters are advected into the SEISAMW formation re-
446 gion. The surface waters experience strong surface cooling before reaching the southeast
447 Indian Ocean, but the intermediate waters are transported along isopycnals while trans-
448 forming into the SEISAMW. This emphasizes the importance of lateral advection in the
449 SEISAMW formation.

450 Eddies and topography play an important role in watermass exchange between ocean
451 sectors. “Hot-spots” of exchange are associated with major seamounts. Enhanced cross-
452 ACC transport occurs around the Agulhas and Crozet Plateaus and particularly just
453 downstream of the KP. The exchange downstream of the KP is so great that “hot-
454 spots” of mixing that are further downstream, such as the Macquarie Ridge and the
455 Campbell Plateau, become insignificant for redistributing the tracers originating in the
456 Agulhas current. The fraction of Agulhas waters transported into and across the ACC
457 is small compared with the Agulhas current transport itself; however, the accumulated
458 modest transport of Agulhas waters towards Antarctica could have significant climatic
459 implications as the heat and salt gradients between the subtropics and the polar oceans
460 are substantial.

Appendix A: Quantification of pathway branches

461 Quantification of pathway branches is accomplished by dividing the domain into 16
462 sectors based on the position of the two main pathways (white lines in Figure 7), the
463 mean SSH streamlines, and two meridional lines separating the Atlantic, Indian and
464 Pacific Ocean basins. Refer to Figure 14 for the structure and specific values used for
465 defining the 16 sectors. The ensemble mean of the percentage of tracer content entering
466 each sector is presented in Figure 13. The ensemble standard deviation is also given
467 as an estimate of the uncertainty. The uncertainty estimate is approximate due to the
468 limited ensemble size of 6 releases, but serves as an adequate guideline. The numbers
469 given in Figure 13 represent the pathway branches deemed most important for meridional
470 property redistribution. Numbers for the Pacific are omitted due to the fact that after the
471 three-year simulation they are insignificant. Numbers for the mean pathway are omitted
472 as they are sensitive to the choice of the sector bounds.

473 **Acknowledgments.** We acknowledge the National Science Foundation (NSF) for sup-
474 port of this research through grants OCE-1234473 and OPP-0961218. SOSE was pro-
475 duced using the Extreme Science and Engineering Discovery Environment (XSEDE),
476 which is supported by National Science Foundation grant number MCA06N007. We
477 thank Lynne Talley and Ivana Cerovečki for helpful conversations. Comments from two
478 reviewers and Veronica Tamsitt helped improve the manuscript. The data used in this
479 study are available at sose.ucsd.edu. Additional relevant movies can be found at [www-](http://www-pord.ucsd.edu/~jinbo/main/)
480 pord.ucsd.edu/~jinbo/main/.

References

- 481 Beal, L. M. (2009), A time series of Agulhas Undercurrent transport, *J. Phys. Oceanogr.*,
482 *39*(10), 2436–2450, doi:10.1175/2009JPO4195.1.
- 483 Beal, L. M., and H. L. Bryden (1999), The velocity and vorticity structure of the Agulhas
484 Current at 32S, *J. Geophys. Res.*, *104*(C3), 5151–5176, doi:10.1029/1998JC900056.
- 485 Beal, L. M., T. K. Chereskin, Y. D. Lenn, and S. Elipot (2006), The sources and mixing
486 characteristics of the Agulhas Current, *J. Phys. Oceanogr.*, *36*(11), 2060–2074, doi:
487 10.1175/JPO2964.1.
- 488 Beal, L. M., W. P. M. De Ruijter, A. Biastoch, and R. Zahn (2011), On the role of the
489 Agulhas system in ocean circulation and climate., *Nature*, *472*(7344), 429–436, doi:
490 10.1038/nature09983.
- 491 Belkin, I. M., and A. L. Gordon (1996), Southern Ocean fronts from the Greenwich
492 meridian to Tasmania, *J. Geophys. Res.*, *101*(C2), 3675–3696, doi:10.1029/95JC02750.
- 493 Biastoch, A., and C. W. Böning (2013), Anthropogenic impact on Agulhas leakage, *Geo-*
494 *phys. Res. Lett.*, *40*(6), 1138–1143, doi:10.1002/grl.50243.
- 495 Biastoch, A., and W. Krauss (1999), The role of mesoscale eddies in the source regions of
496 the Agulhas Current, *J. Phys. Oceanogr.*, *29*(9), 2303–2317.
- 497 Biastoch, A., C. W. Böning, F. U. Schwarzkopf, and J. R. E. Lutjeharms (2009a), Increase
498 in Agulhas leakage due to poleward shift of Southern Hemisphere westerlies., *Nature*,
499 *462*(7272), 495–498, doi:10.1038/nature08519.
- 500 Biastoch, A., L. M. Beal, J. R. E. Lutjeharms, and T. G. D. Casal (2009b), Variability and
501 coherence of the Agulhas Undercurrent in a high-resolution ocean general circulation
502 model, *J. Phys. Oceanogr.*, *39*(10), 2417–2435, doi:10.1175/2009JPO4184.1.

- 503 Boebel, O., J. Lutjeharms, C. Schmid, W. Zenk, T. Rossby, and C. Barron (2003), The
504 Cape Cauldron: a regime of turbulent inter-ocean exchange, *Deep Sea Res. Part II Top.*
505 *Stud. Oceanogr.*, *50*(1), 57–86, doi:10.1016/S0967-0645(02)00379-X.
- 506 Bryden, H. L., L. M. Beal, and L. M. Duncan (2005), Structure and transport of
507 the Agulhas Current and its temporal variability, *J. Oceanogr.*, *61*(3), 479–492, doi:
508 10.1007/s10872-005-0057-8.
- 509 Caley, T., J. Giraudeau, B. Malaizé, L. Rossignol, and C. Pierre (2012), Agulhas leakage
510 as a key process in the modes of Quaternary climate changes., *Proc. Natl. Acad. Sci.*
511 *U. S. A.*, *109*(18), 6835–9, doi:10.1073/pnas.1115545109.
- 512 Cerovečki, I., L. D. Talley, and M. R. Mazloff (2011), A comparison of Southern Ocean
513 air-sea buoyancy flux from an ocean state estimate with five other products, *J. Clim.*,
514 *24*(24), 6283–6306, doi:10.1175/2011JCLI3858.1.
- 515 Cerovečki, I., L. D. Talley, M. R. Mazloff, and G. Maze (2013), Subantarctic Mode Wa-
516 ter formation, destruction, and export in the eddy-permitting Southern Ocean State
517 Estimate, *J. Phys. Oceanogr.*, *43*(7), 1485–1511, doi:10.1175/JPO-D-12-0121.1.
- 518 Firing, Y. L., T. K. Chereskin, and M. R. Mazloff (2011), Vertical structure and transport
519 of the Antarctic Circumpolar Current in Drake Passage from direct velocity observa-
520 tions, *J. Geophys. Res.*, *116*(C8), C08,015, doi:10.1029/2011JC006999.
- 521 Gordon, A. L. (1986), Interocean exchange of thermocline water, *J. Geophys. Res.*,
522 *91*(C4), 5037–5046, doi:10.1029/JC091iC04p05037.
- 523 Griesel, a., M. R. Mazloff, and S. T. Gille (2012), Mean dynamic topography in the
524 Southern Ocean: Evaluating Antarctic Circumpolar Current transport, *J. Geophys.*
525 *Res.*, *117*(C1), C01,020, doi:10.1029/2011JC007573.

- 526 Harris, T. (1972), Sources of the Agulhas current in the spring of 1964, *Deep Sea Res.*
527 *Oceanogr. Abstr.*, 19(9), 633–650, doi:10.1016/0011-7471(72)90091-5.
- 528 Large, W. G., and S. G. Yeager (2009), The global climatology of an interannually varying
529 air-sea flux data set, *Clim. Dyn.*, 33, 341–364, doi:10.1007/s00382-008-0441-3.
- 530 Lutjeharms, J., and I. Ansorge (2001), The Agulhas Return Current, *J. Mar. Syst.*, 30(1-
531 2), 115–138, doi:10.1016/S0924-7963(01)00041-0.
- 532 Lutjeharms, J. R. E. (1976), The Agulhas Current System during the northeast monsoon
533 season, *J. Phys. Oceanogr.*, 6(5), 665–670.
- 534 Marshall, J., and K. Speer (2012), Closure of the meridional overturning circulation
535 through Southern Ocean upwelling, *Nat. Geosci.*, 5(3), 171–180, doi:10.1038/ngeo1391.
- 536 Mazloff, M. R. (2012), On the sensitivity of the Drake Passage transport to air-sea mo-
537 mentum flux, *J. Clim.*, 25(7), 2279–2290, doi:10.1175/JCLI-D-11-00030.1.
- 538 Mazloff, M. R., P. Heimbach, and C. Wunsch (2010), An Eddy-permitting southern ocean
539 state estimate, *J. Phys. Oceanogr.*, 40(5), 880–899, doi:10.1175/2009JPO4236.1.
- 540 McCartney, M. S. (1982), The subtropical recirculation of mode waters, *J. Mar. Res.*, 40,
541 427–464.
- 542 Orsi, A. H., T. Whitworth, and W. D. Nowlin (1995), On the meridional extent and fronts
543 of the Antarctic Circumpolar Current, *Deep Sea Res. Part I Oceanogr. Res. Pap.*, 42(5),
544 641–673, doi:10.1016/0967-0637(95)00021-W.
- 545 Pavlis, N. K., S. a. Holmes, S. C. Kenyon, and J. K. Factor (2012), The development
546 and evaluation of the Earth Gravitational Model 2008 (EGM2008), *J. Geophys. Res.*,
547 117(B4), B04,406, doi:10.1029/2011JB008916.

- 548 Pollard, R. T., and J. F. Read (2001), Circulation pathways and transports of the Southern
549 Ocean in the vicinity of the Southwest Indian Ridge, *J. Geophys. Res.*, *106*(C2), 2881,
550 doi:10.1029/2000JC900090.
- 551 Richardson, P. L. (2007), Agulhas leakage into the Atlantic estimated with subsurface
552 floats and surface drifters, *Deep Sea Res. Part I Oceanogr. Res. Pap.*, *54*(8), 1361–
553 1389, doi:10.1016/j.dsr.2007.04.010.
- 554 Roquet, F., Y.-H. Park, C. Guinet, F. Bailleul, and J.-B. Charrassin (2009), Observations
555 of the Fawn Trough Current over the Kerguelen Plateau from instrumented elephant
556 seals, *J. Mar. Syst.*, *78*(3), 377–393, doi:10.1016/j.jmarsys.2008.11.017.
- 557 Sallée, J.-B., N. Wienders, K. Speer, and R. Morrow (2006), Formation of Subantarctic
558 Mode Water in the Southeastern Indian Ocean, *Ocean Dyn.*, *56*(5-6), 525–542, doi:
559 10.1007/s10236-005-0054-x.
- 560 Sallée, J.-B., K. G. Speer, and S. R. Rintoul (2010), Zonally asymmetric response of the
561 Southern Ocean mixed-layer depth to the Southern Annular Mode, *Nat. Geosci.*, *3*(4),
562 273–279, doi:10.1038/ngeo812.
- 563 Talley, L. D., G. L. Pickard, W. J. Emery, and J. H. Swift (2011), *Descriptive Physical*
564 *Oceanography: An Introduction*, 560 pp., Academic Press.
- 565 Thompson, A. F., P. H. Haynes, C. Wilson, and K. J. Richards (2010), Rapid Southern
566 Ocean front transitions in an eddy-resolving ocean GCM, *Geophys. Res. Lett.*, *37*(23),
567 L23,602, doi:10.1029/2010GL045386.
- 568 van Sebille, E., P. J. van Leeuwen, A. Biastoch, and W. P. de Ruijter (2010a), Flux
569 comparison of Eulerian and Lagrangian estimates of Agulhas leakage: A case study
570 using a numerical model, *Deep Sea Res. Part I Oceanogr. Res. Pap.*, *57*(3), 319–327,

571 doi:10.1016/j.dsr.2009.12.006.

572 van Sebille, E., P. J. van Leeuwen, A. Biastoch, and W. P. M. de Ruijter (2010b),

573 On the fast decay of Agulhas rings, *J. Geophys. Res.*, *115*(C3), C03,010, doi:

574 10.1029/2009JC005585.

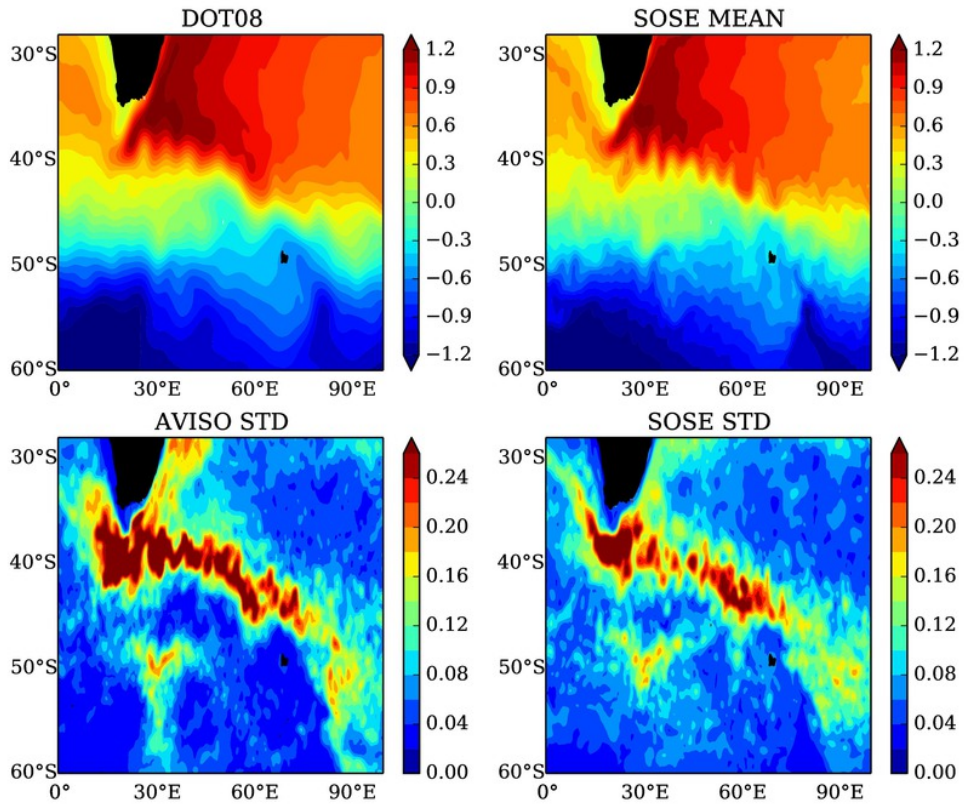


Figure 1. The mean dynamic topography (meter) from DOT08 [Pavlis *et al.*, 2012] (top left), and from the three-year (2008-2010) SOSE solution (top right). The standard deviation of SSH from the AVISO objectively mapped product (bottom left) and from the SOSE solution (bottom right) for 2008-2010.

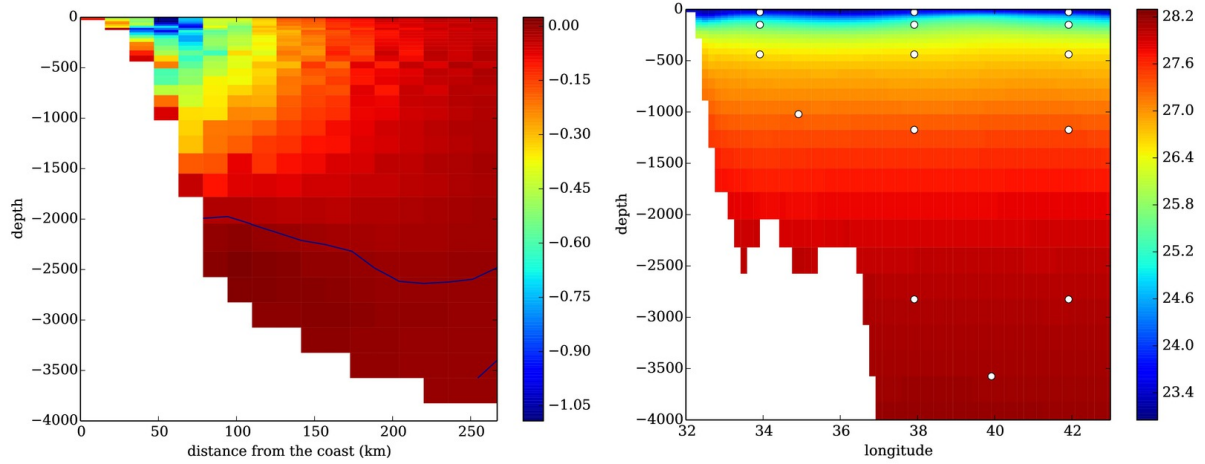


Figure 2. Left: the three-year-mean meridional velocity at 32°S. The line marks the zero velocity contour. Right: Section showing neutral density at 29°S from 32°E to 43°E. Tracer #1 fills the whole section. The centers of the other fifteen localized tracers are marked by the white dots. Note that the latitude of the sections and the x-axis is different in two panels.

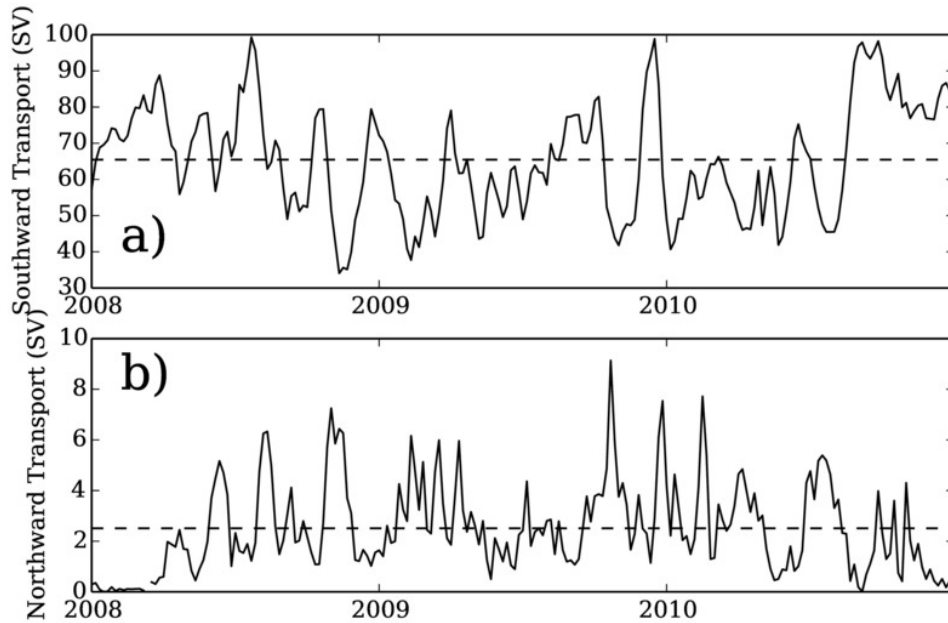


Figure 3. The time series of southward (a) and northward (b) transport integrated over 204 km off the coast at 32°S. $1 \text{ Sv} = 10^6 \text{ m}^3 \text{ s}^{-1}$.

Acronym	Temperature(°C)	Salinity (psu)	Potential Density (kg m ⁻³)
SAMW	4-15	34.2-35.8	26.5-27.1
SEISAMW	8	34.55	26.8
AAIW	4.7	34.39	27.2
IOSTMW	17-18	35.6	26.0

Table 1. Mode waters discussed in the paper following the convention in *Talley et al.* [2011]. The listed watermasses are Sub-Antarctic Mode Water (SAMW), Southeast Indian SAMW (SEISAMW), Antarctic Intermediate Water (AAIW), and Indian Ocean Sub-Tropical Mode Water (IOSTMW).

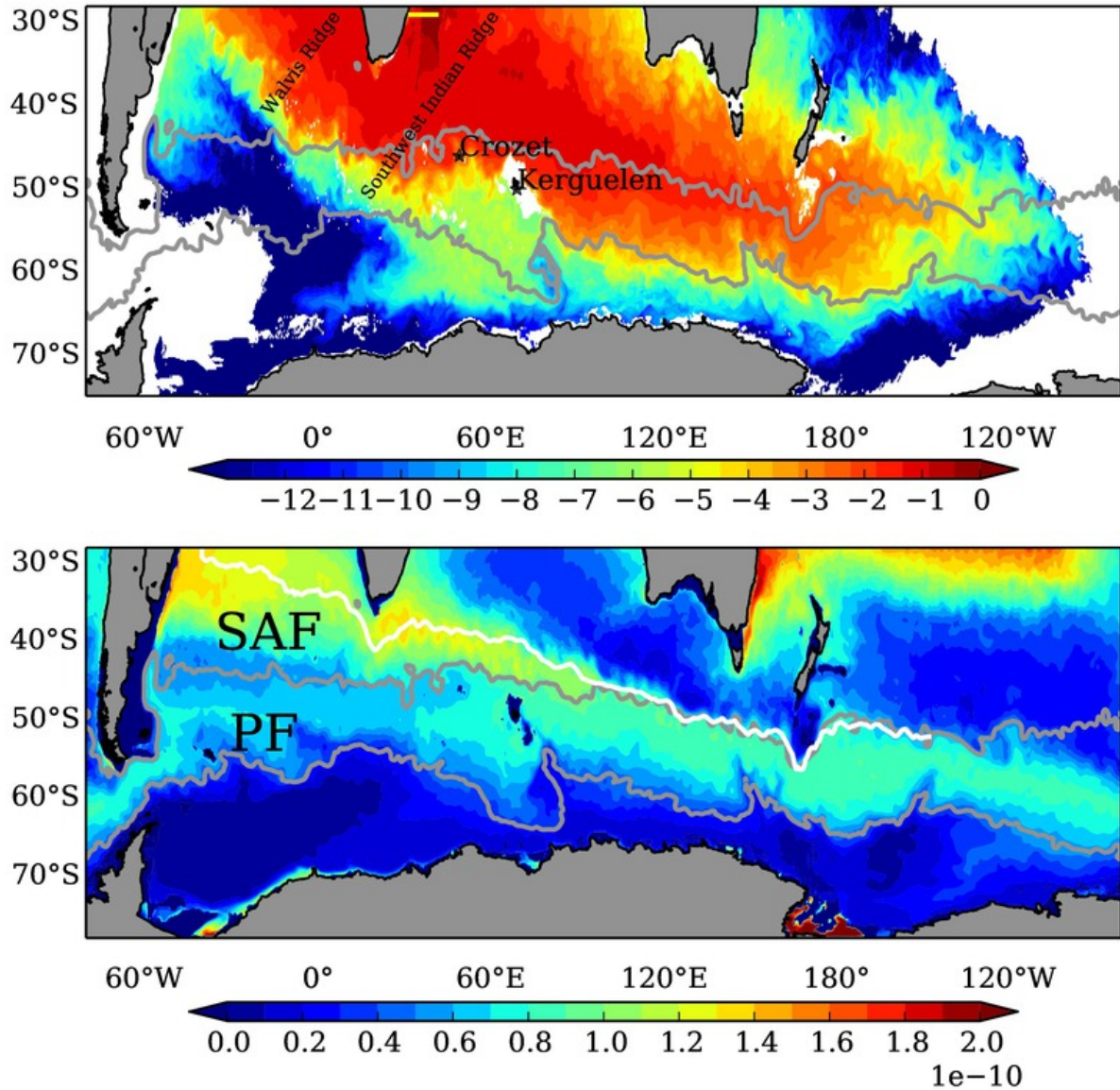


Figure 4. Upper: the vertically integrated and time-averaged tracer content in a \log_{10} scale (color) for the year 2010. The tracer is initially released in a band at 29°S within an 11° longitude range extending from the South African continent to 42°E (the yellow bar) and from the surface to the bottom. The gray lines divide the SOSE domain into nine sections. The more zonally-oriented curved gray lines are vertically integrated transport streamlines: 20 Sv to the south and 140 Sv to the north. Thick white lines are the 3000 meters isobath. Lower: the potential vorticity ($f\rho^{-1}\partial\rho/\partial z$) at 500 m averaged over three years. The white line marks the main pathway of the intermediate tracer (around 500 m)

as shown in Figure 7.
D R A F T

June 12, 2014, 11:31pm

D R A F T

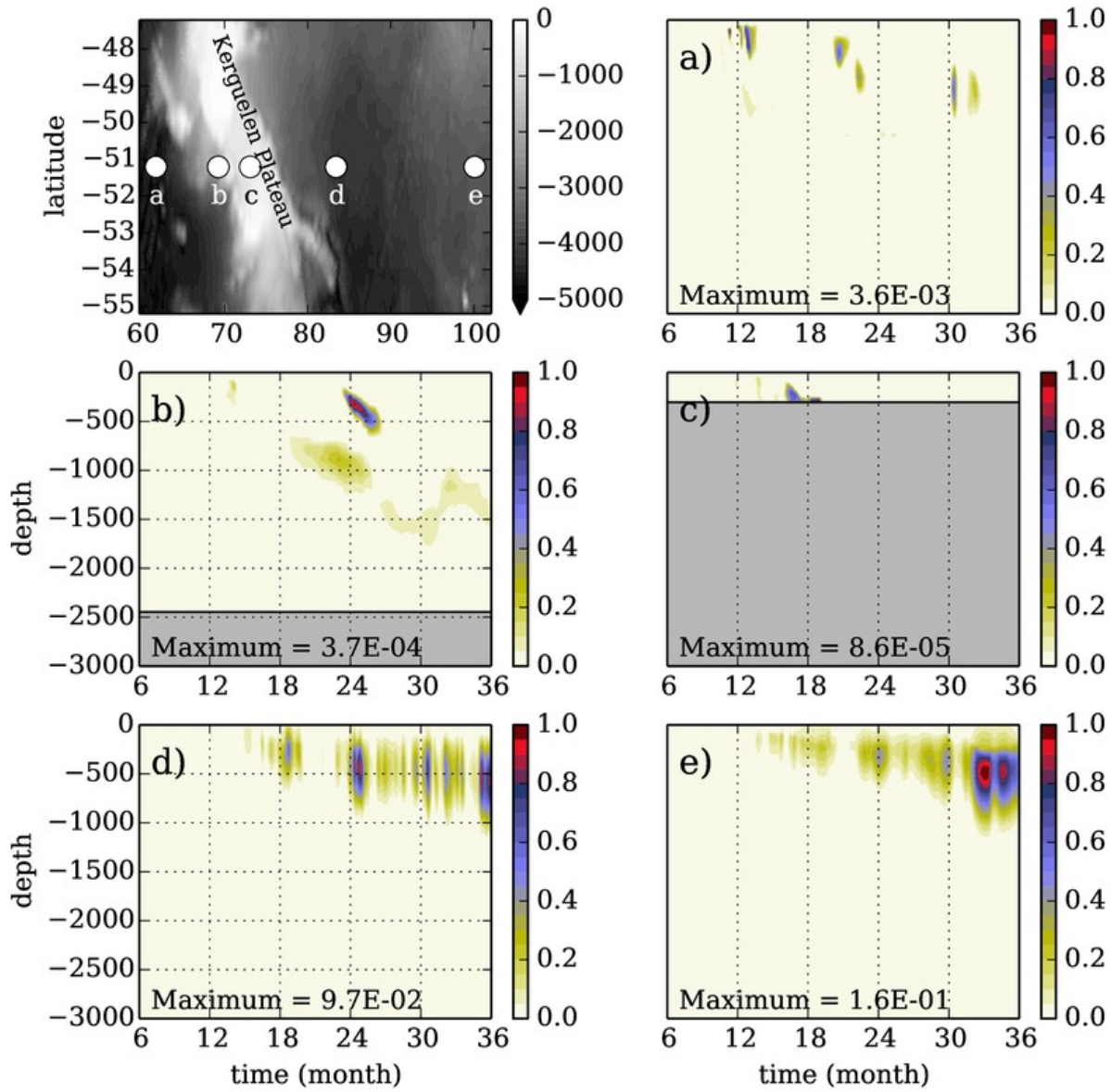


Figure 5. The upper left panel shows the depth of the ocean bottom for the region over the KP. The white dots mark five locations for which the Hovmöller diagram of the vertical profile of the tracer concentration is shown in panel a-e. The tracer concentration in each panel is normalized by the maximum value noted at the bottom. The levels below sea floor are shaded gray.

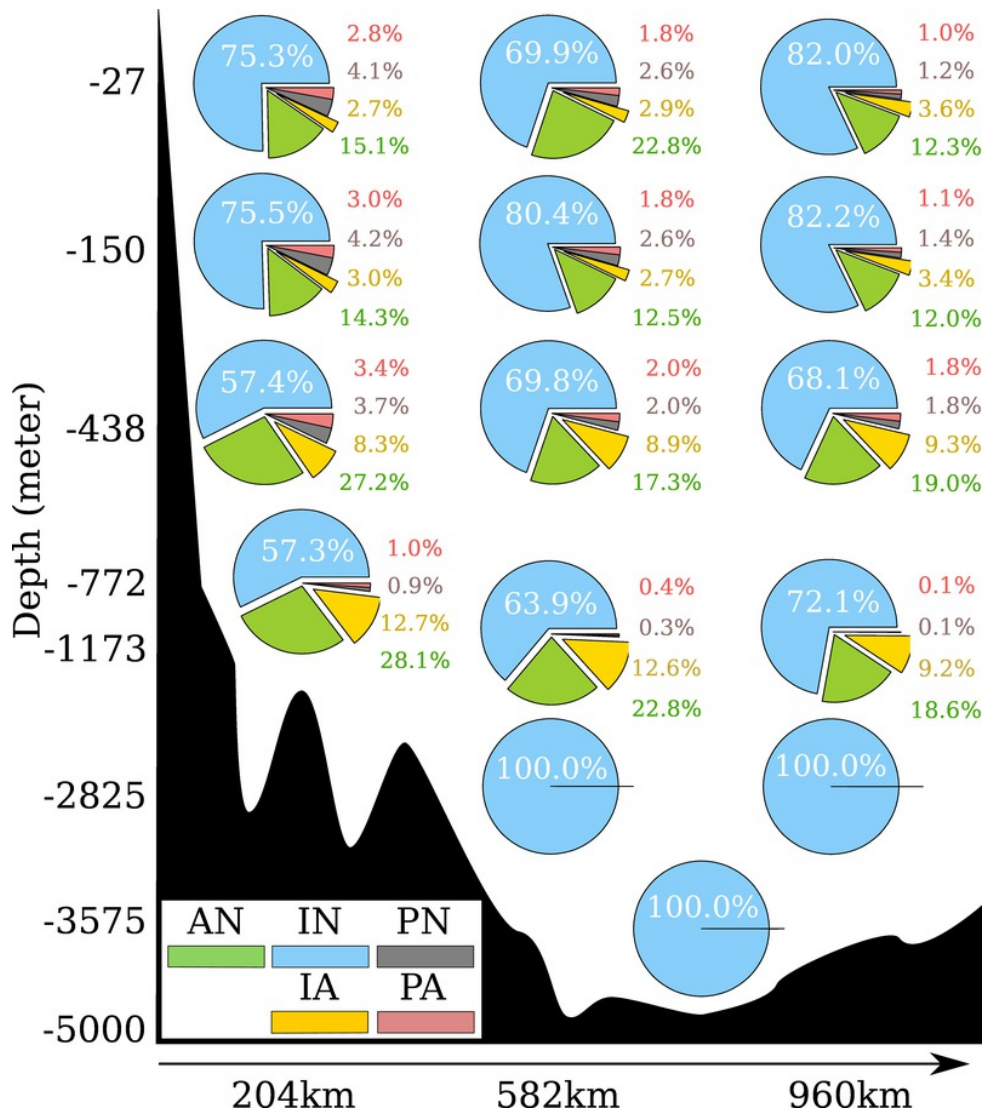


Figure 6. Final tracer distributions into five main ocean sectors (color-coded) for fifteen initial Gaussian tracer patch releases, represented by pie charts, at different depths (y-axis) and offshore locations (x-axis). The ocean sectors are denoted as AN, IN, PN to represent sections north of the ACC in the Atlantic, Indian, and Pacific Oceans, respectively. The IA and PA denote the ACC in the Indian Ocean and Pacific Ocean, respectively. The depth-coordinate is stretched to accommodate all the pie charts.

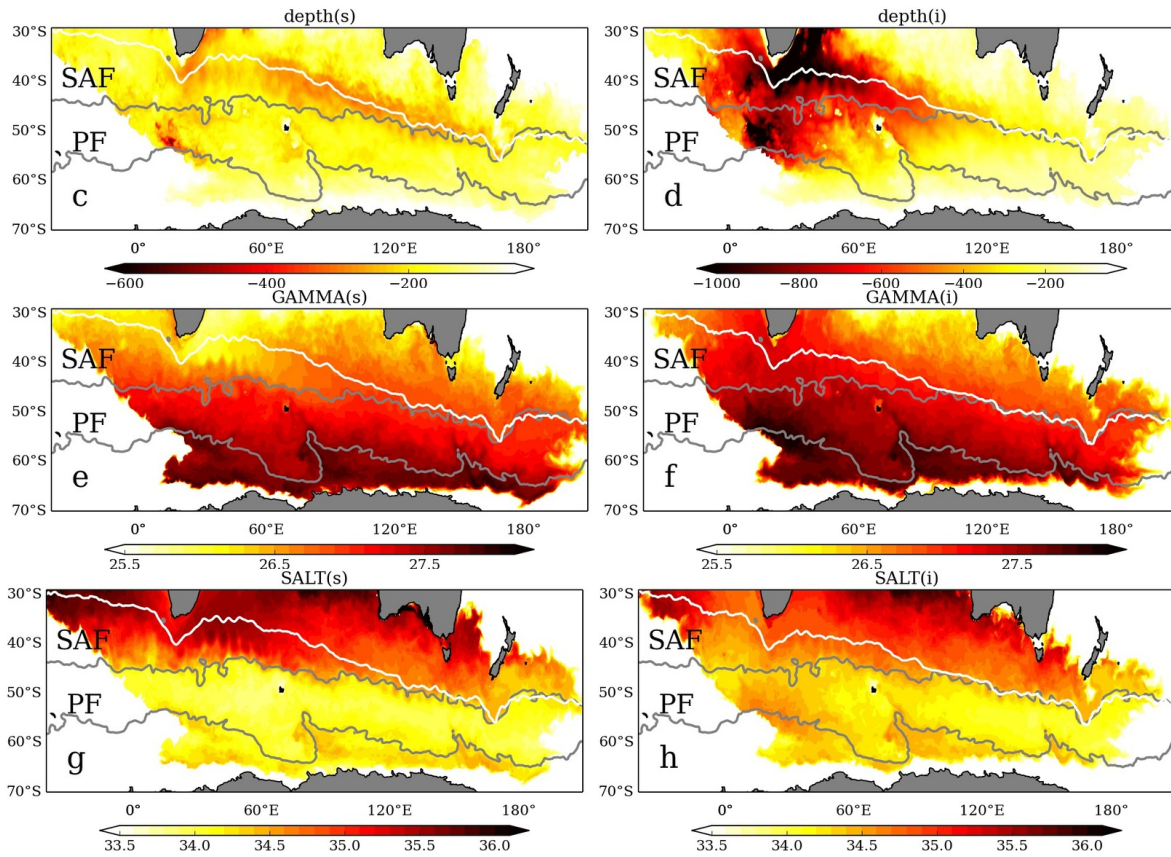


Figure 7. The surface (a) and intermediate (b) tracer concentrations averaged for the final year plotted on a logarithmic scale. The center of the surface (left columns) and intermediate (right columns) tracer depth (c,d), neutral density (e,f), and salinity (g,h). The white lines mark the main tracer pathways for the intermediate tracer (right panels) and surface tracer (left panels) defined by y_c in Eq. 1. Two gray lines are the same as in Figure 4 denoting SAF and PF.

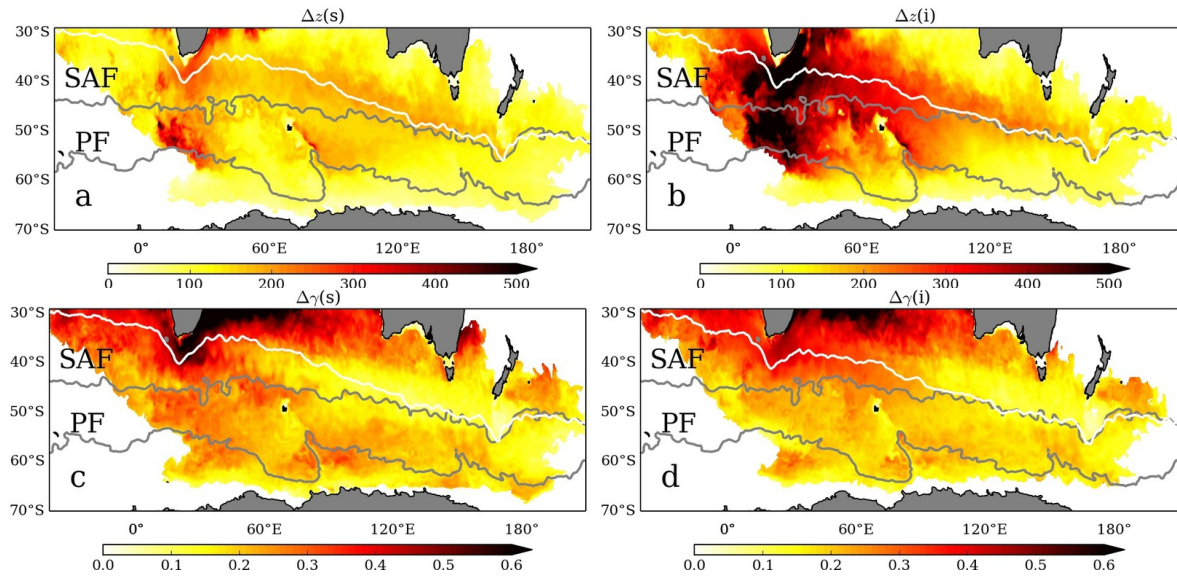


Figure 8. The surface (a,c) and intermediate (b,d) tracer thickness in depth (meter) (a,b) and density (kg m^{-3}) space (c,d). The white and gray lines are the same as in Figure

7

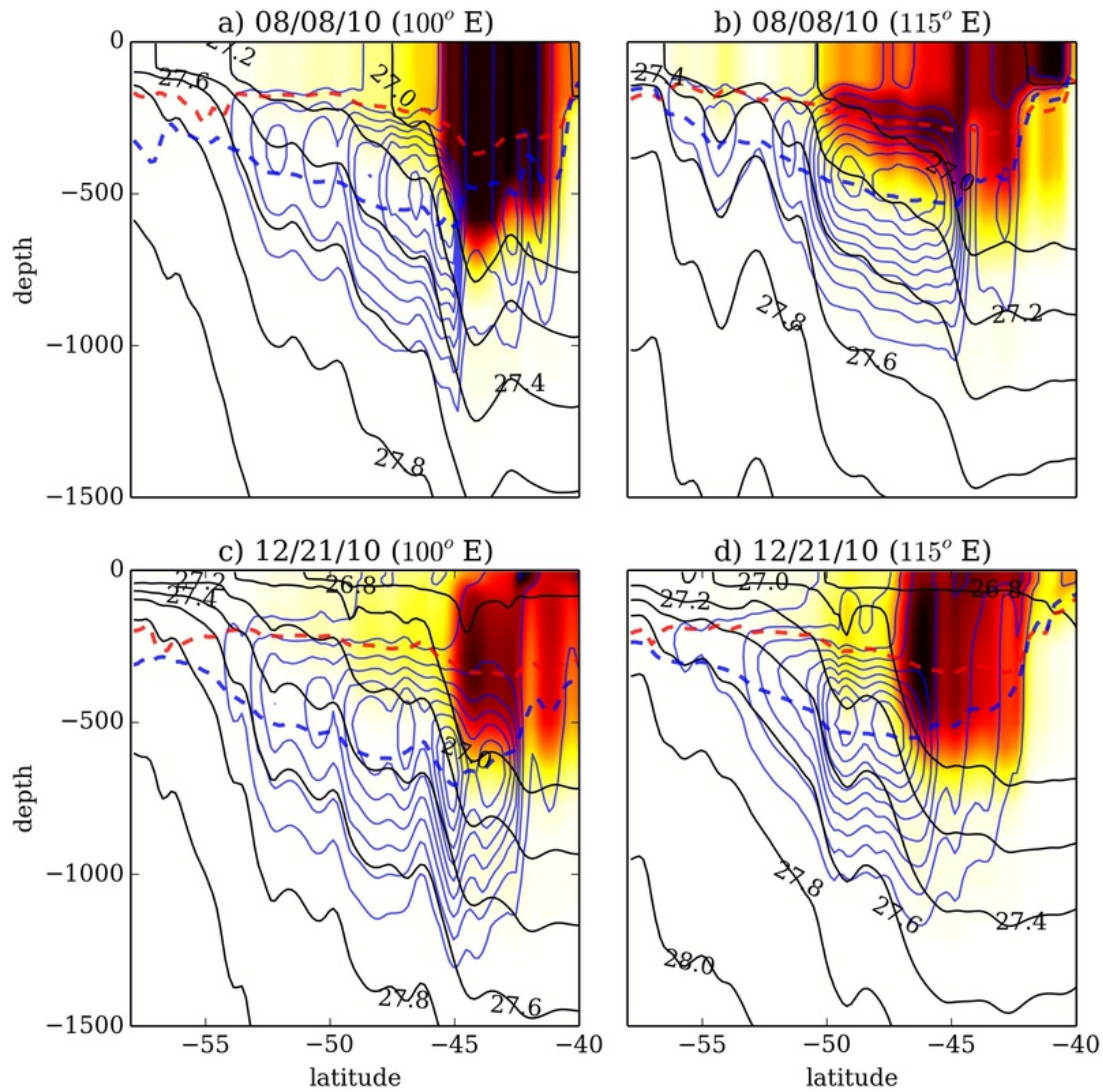


Figure 9. Cross sections of the five-day-averaged concentration of a surface tracer (color) and an intermediate tracer (blue contour) along 100°E (a,c) and 115°E (b,d) during 8/8/2010, the austral winter (a,b), and 12/21/2010, the austral summer (c,d). The black contours show the instantaneous neutral density (kg m^{-3}). The dashed lines mark the first moment in z for the surface (red) and intermediate (blue) tracers. The approximate latitudes of the (SAF, PF) defined by the temperature front at 200 meters (thresholds: 2.5°C for the PF and 6°C for the SAF) are (48°S,53°S), (50°S,57°S), (49°S,54°S), and (51°S,57°S), for (a), (b), (c), and (d), respectively. Note that large uncertainties exist due to the distortion of isotherms by instantaneous energetic eddies.

Figure 10. The net surface heat flux (W m^{-2}) experienced by Tracer #1 during the first 7 months (a) and the last 12 months (b). Negative values represent ocean heat loss.

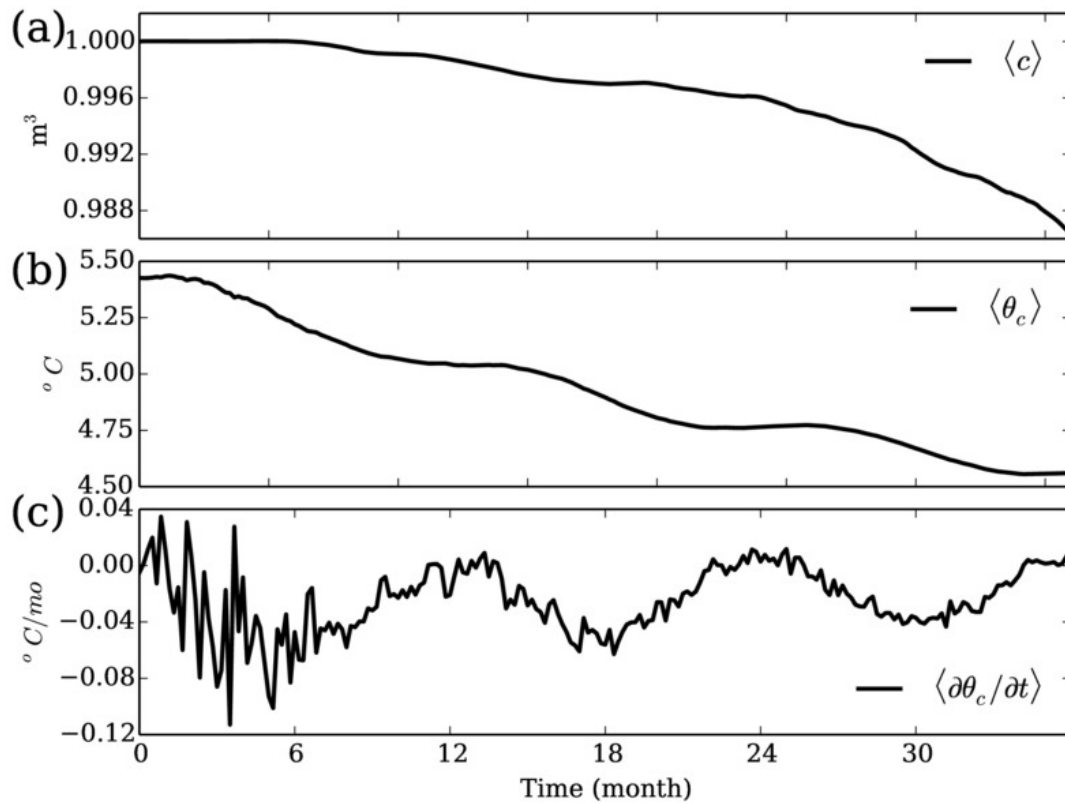


Figure 11. The evolution of tracer content normalized by the initial value (a), tracer temperature (in $^{\circ}\text{C}$) (b), time tendency of the tracer temperature $^{\circ}\text{C}/\text{month}$ (c).

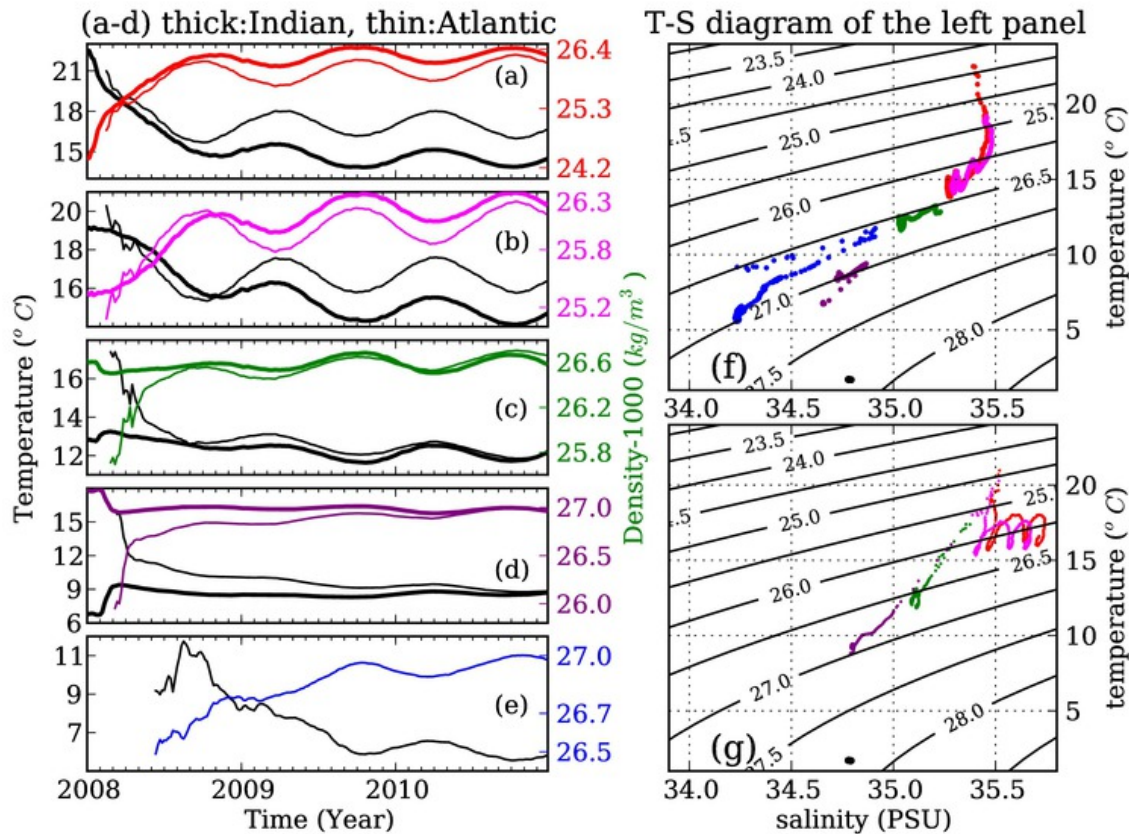


Figure 12. Evolution of four watermasses (color-coded consistently in all panels) shown as time series (left panel) and in a potential temperature-salinity diagram (right). Panels (a)-(d) correspond to tracers initially released at 27, 150, 438, 772 meters, respectively. Colored lines represent tracer-weighted density, and black lines potential temperature. The thick lines in (a)-(d) represent tracer found in the Indian Ocean north of the ACC, and the thin lines represent tracer found in the South Atlantic north of the ACC. Panel (e) shows tracer weighted density (blue) and temperature (black) in Indian sector of the ACC. The right panel shows the same data but in a T-S diagram. Panels (f) and (g) represent the thick lines and thin lines in (a-d), respectively. The blue dots in (f) correspond to the blue line in (e). In addition, the tracer released around 2825 meters is shown in the right panel with black dots. These dots cluster at (34.8, 1.7°C) indicating the stagnation

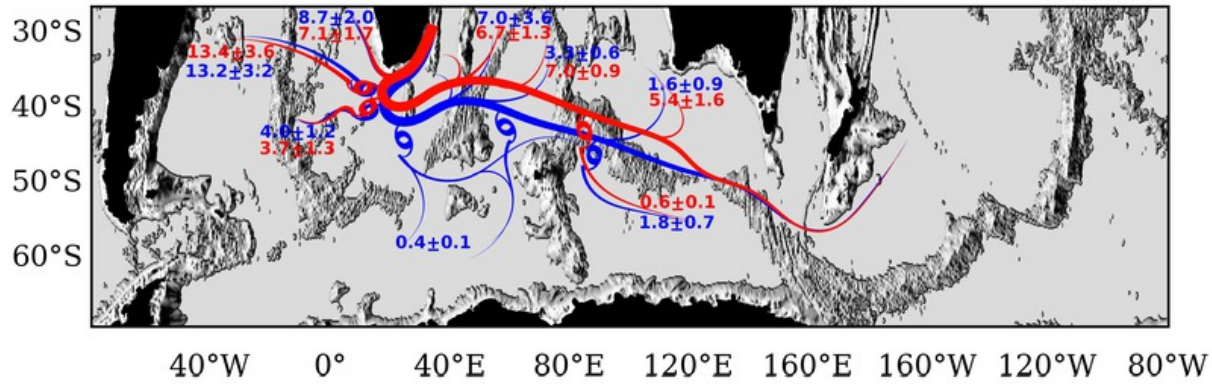


Figure 13. A schematic of the Agulhas water pathways. Bathymetry is in black-gray colors. Red color represents the tracers released in the upper layer of the Agulhas Current (the upper 400 meters). The blue colors represent the intermediate tracers released between 400 and 1500 meters. Numbers show the ensemble-averaged percentage of the tracer in each subdomain branch averaged in 2010 with standard deviation as uncertainties. The remaining percentage, 56.1% for the surface tracers and 60% for the intermediate tracers, still resides in the main pathway. Spirals represent the location of enhanced stirring, inferred by large variations in properties. The main pathway of the tracer is meridionally shifted between surface and intermediate layer, which is due to the northward surface Ekman flow. Refer to the Appendix for details on the creation of this schematic.

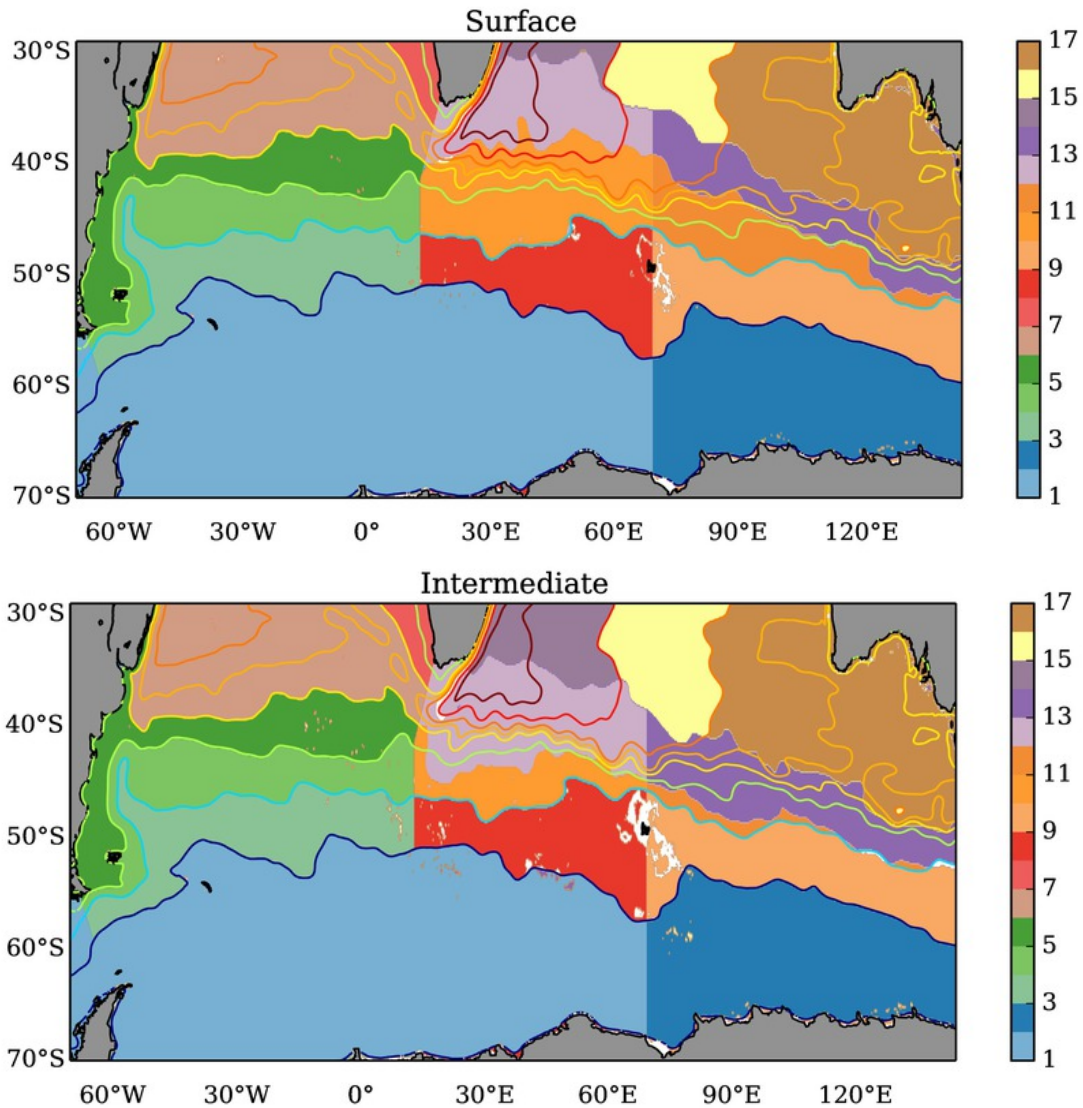


Figure 14. Color-coded 16 sectors used in quantifying the tracer pathways shown in Figure 13. The upper panel is for surface layer releases and the lower panel is for the intermediate layer releases with the primary difference being in the location of the main pathway. The contours show the three-year-averaged SSH. The SSH contour levels are $[-0.8, -0.2, 0.2, 0.4, 0.5, 0.6, 0.8, 1.0]$ starting from south. The levels -0.8m and -0.2m approximate the 20 Sv and 140 Sv vertically integrated transport streamlines and denote the boundaries of the main ACC core. Regions 12 and 13 are the main tracer pathways shown in Figure 7, divided by the 70°E meridian crossing the KP. The time-averaged tracer budget in 2010 is quantified for these 16 sectors and presented schematically in